Investigations on Thermoacoustic Feedback on a Representative Test Chamber Configuration

By A. Urbano†, M. Schulze‡, M. Zahn‡, M. Schmid‡, T. Sattelmayer‡ AND M. Oschwald¶

† Dipartimento di Ingegneria Meccanica e Aerospaziale, Sapienza University of Rome, Via Eudossiana 18, 00184 Roma
‡ Lehrstuhl für Thermodynamik, Technische Universität München Boltzmannstr. 15, 85748 Garching b. München
¶ Deutches Zentrum für Luft- und Raumfahrt (DLR), Institute für Raumfahrtantriebe Lampoldshausen, Langer Grund, 74239 Hardthausen

Combustion instabilities represent a challenging problem affecting a large number of rocket engine combustion chambers. Aim of the present study is to test a numerical procedure to predict the linear stability of an acoustic mode in a three dimensional configuration. The reference configuration is the BKD combustion chamber from the "Deutsches Zentrum für Luft- und Raumfahrt Lampoldshausen", which shows self-excited combustion instabilities for the first tangential mode for certain load points. Here, four given load points are numerically investigated in terms of their stability behavior. For each load point, a flame transfer function around the first tangential mode frequency is determined from numerical simulations of a single injector. Moreover, a three dimensional mean flow in the combustion chamber is computed considering equilibrium conditions in the chamber. Finally, mean flow and response function are introduced into the linearized Euler code PIANO to analyze the thermoacoustic feedback. Results show that the methodology is able to perform a complete stability analysis from only the knowledge of the load point conditions by predicting the growth rates.

1. Introduction

Combustion instabilities have been investigated since the beginning of rocket engine development [2–4]. To be stable, the combustion system has to prove its ability to damp sudden heavy but temporary forcing, e.g. a major incident in the combustion process within a certain time span. For too high acoustic amplitudes and insufficient damping, the combustion system is declared as unstable and is thus highly prone to suffer major failures during operation. The consideration of thermoacoustic instabilities is a main task during the design and test process of every rocket engine. To overcome such instabilities in the final stages of the development process is expensive but necessary. Therefore, appropriate methods to indicate the potential for thermoacoustic instabilities need to be applied from the beginning of a new engine design and used in an iterative process during the entire development process. However, thermoacoustic instability can only be investigated on full-scale level, which makes experimental procedures very expensive and tedious. Thus, numerical approaches are promising for both high-quality and efficient stability predictions.

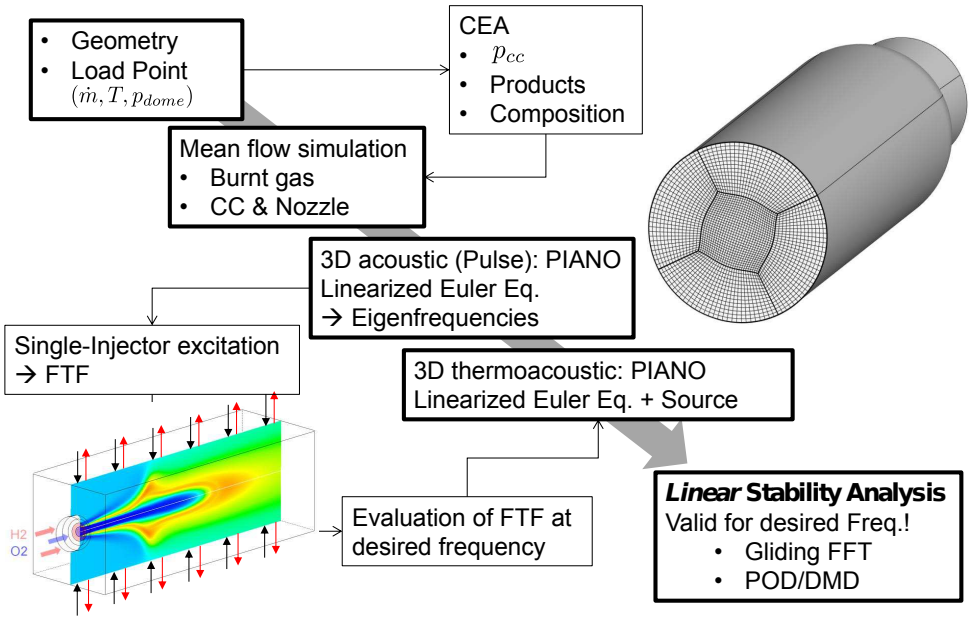

FIGURE 1. Coupled numerical methodology to predict the linear thermoacoustic stability.

In the present study a coupled numerical procedure to predict the linear stability of a real combustion chamber configuration, previously presented in [8], is tested. A flow chart that summarizes the procedure is shown in Fig. 1. The only inputs are the geometry and the operative conditions whereas the ultimate goal is the linear stability analysis which is carried out with a linearized Euler Equations (LEE) code called PIANO, including a response function previously evaluated from a single injector unsteady simulation. The first step is to compute the 3D mean flow with a RANS simulation. The mean flow is then used to carry out an acoustic analysis with PIANO to evaluate the first tangential mode frequency. URANS simulations of a single injector are then carried out to evaluate a flame transfer function (FTF) around the frequency of interest, which can be evaluated from the time series of acoustic pressure and heat release rate as:

$$FTF(\omega) = \frac{\hat{q}(\omega)/\bar{q}}{\hat{p}(\omega)/\bar{p}} \tag{1.1}$$

where q is the specific heat release (W/m^3) and p the pressure. Moreover, $\bar{\bullet}$ indicates the mean in time, $'\bullet$ indicates the quantity oscillation with respect to the mean and $\hat{\bullet}$ indicates the Fourier transform. Finally, the FTF at the frequency of interest and the mean flow can be used in the PIANO code to simulate the 3D perturbed field in the whole chamber and therefore to analyze the mode stability. For that purpose, the identified FTF is reduced to the classical n-τ model and evaluated at the frequency of interest for which the stability analysis has to be done.

The particular goal of the project is to analyze the stability of the first transverse (T1) mode of the DLR BKD combustion chamber for different operative conditions. The output time series can be analyzed with a gliding FFT which allows for the determination of decaying or growth rate for a specific acoustic mode and so finally the stability of the configuration can be judged. However, the results are only meaningful for the frequency under consideration. In fact, as shown in [13], a certain confidence region can be derived

in which the stability prediction of the considered configuration is within a tolerable error level.

In the following, the considered test chamber BKD from DLR Lampoldshausen is first presented and a rapid method to estimate the chamber pressure for the given load points (LP) is introduced. The coupled numerical procedure to carry out the linear stability analysis is then explained and details are given for each numerical tool. Results for each step of the procedure are then shown for each load point, that is the evaluation of the first transversal mode frequency, the FTF evaluation and finally the thermoacoustic analysis which permits to judge the BKD stability behavior.

2. The BKD Combustion Chamber

The combustion chamber D (in German ***B**renn**k**ammer **D***) operated at the Institute of Space Propulsion of the German Space Agency (DLR) Lampoldshausen is a fully equipped real rocket engine in a downscaled configuration which operates under typical upper stage engine conditions (thrust level of 25 kN; chamber pressure of 70-80 bar). The BKD cylindrical combustion chamber (diameter: 80 mm, length: 210 mm), the feed and injection system and the nozzle are shown in Fig. 2. The injection system comprises 42 coaxial injectors which provide O_2 and H_2 as propellants. Thermodynamic conditions of O_2 at the injection are of particular interest in this test case because of its supercritical pressure and subcritical temperature [5].

Self-excited instabilities, with acoustic pressure amplitudes up to 10 bar for the first transverse mode, for certain load points, have been experimentally observed [6, 7]. Self-excited amplification can be described with linear theory. Therefore, BKD is a suitable test case to validate the present coupled methodology which is based on linearized Euler Equations. Four experimental load points are considered in the numerical simulations. The corresponding operative conditions, in terms of mass flow rate $\dot{m}$, injection temperatures (T_{H2}, T_{O2}) and dome pressures (p_{H2}, p_{O2}) are reported in Table 1. From these data it is possible to estimate the chamber pressure p_{cc} assuming chemical equilibrium conditions. The throat is choked and therefore the mass flow rate must fulfill the following gas dynamic relation:

$$\dot{m} = \frac{\Gamma p_{cc} A_t}{\sqrt{R T_{cc}}} \tag{2.1}$$

where T_{cc} is the chamber temperature, R is the gas constant, A_t is the throat area and Γ is a function of the specific heat ratio γ (see [21] for more details). For a given pressure level, T_{cc}, Γ and R are evaluated with the CEA software [22]. The iterative procedure, schematically reported in Fig. 3, is established varying the input chamber pressure for CEA until the properties of the combustion products are such that the throat mass flow given by Eq. (2.1) match the injected mass flow rate. The estimated chamber pressures are reported in the Table 2.

3. Coupled numerical procedure

The coupled numerical procedure that is used in the present study has been introduced in Section 1 (see Fig. 1). In the present section, the numerical models used in each step of the procedure are introduced. Three different models are used to compute the mean flow field, to carry out unsteady simulations of the single injector and for the thermoacoustic analysis.

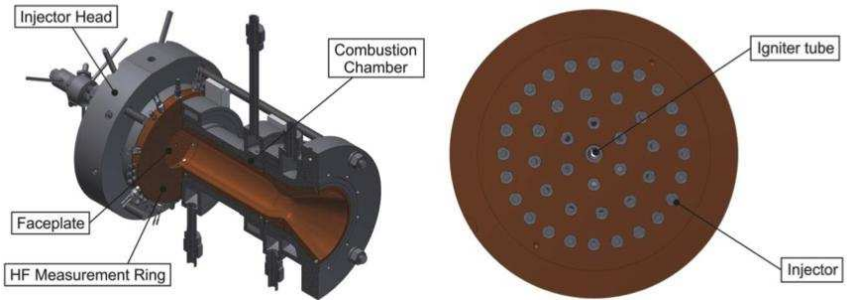

FIGURE 2. Left: DLR's BKD combustion chamber configuration. Right: BKD injector pattern [5].

	LP1	**LP2**	**LP3**	**LP4**
$\dot{\boldsymbol{m}}_{\mathbf{H2}}$ [kg/s]	1,11	0.84	0.96	0.96
$\dot{\boldsymbol{m}}_{\mathbf{O2}}$ [kg/s]	4,44	5,04	5,77	5,75
ROF	4	6	6	6
$\boldsymbol{T}_{\mathbf{H2}}$ [K]	111,80	112,77	79,74	113,38
$\boldsymbol{T}_{\mathbf{O2}}$ [K]	126,46	126,21	123,06	126,16
$\boldsymbol{p}_{\mathbf{H2}}$ [bar]	100,03	89,66	90,12	102,92
$\boldsymbol{p}_{\mathbf{O2}}$ [bar]	78,41	81,11	91,89	94,10

TABLE 1. Experimental data for 4 loads points (LP) [5].

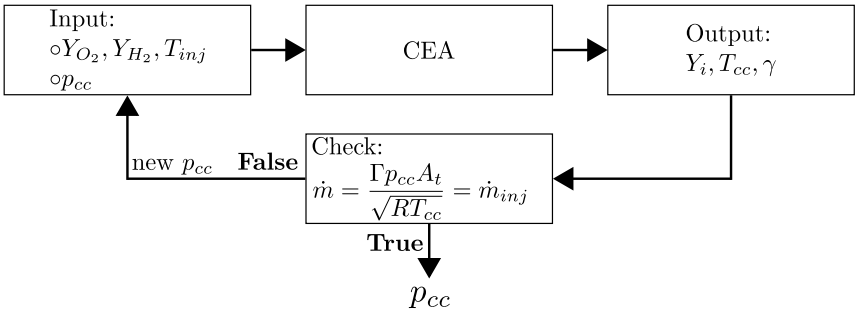

FIGURE 3. Iterative procedure to evaluate chamber pressure for the given experimental data.

3.1. *Mean flow evaluation*

In the first step of the coupled procedure the full set of the three-dimensional multi-component Navier-Stokes equations are solved with the ANSYS CFX commercial code, considering a standard RANS $k-\varepsilon$ turbulence model, to obtain the 3D meanflow field. The computational domain, which is shown in Fig. 4, is restricted to the cylindrical combustion chamber and the nozzle. The domain is discretized with a total number of 900.000 nodes, which provide low computational time. Equilibrium conditions are assumed in the whole domain (non-reacting flow) and conditions evaluated with the CEA software are enforced at the inlet. The walls are treated as adiabatic slip boundaries. At the outlet supersonic conditions are used.

	LP1	**LP2**	**LP3**	**LP4**
$\boldsymbol{p_{CC}}$ [bar]	70,12	70,00	80,22	80,04

TABLE 2. Evaluated chamber pressure from experimental data of Table 1

3.2. *Single injector simulations*

The determination of the FTF is performed with single-injector unsteady simulations (see [10, 12] for more details). Unsteady RANS simulations with $k-\varepsilon$ turbulence modelling and the Eddy Dissipation Model to account for the combustion process are carried out with the commercial solver ANSYS CFX and the system is excited in the frequency range of interest. The global reaction $\frac{1}{2}O_2 + H_2 \rightarrow H_2O$ is considered in the Eddy Dissipation Model.

The computational domain, shown in Fig. 6, is 2D axi-symmetrical, and has the combustion chamber length and a diameter corresponding to 1/42 of the chamber cross-section. Additionally, the recess length of the injector is considered. At the inlet, constant mass flows of the propellants and their injection temperatures are applied. At the slip walls source terms of mass with the local composition of the calculated species are added to establish the acoustic perturbation at the frequency of interest. At the outlet the chamber pressure is enforced. This way of exciting a single-injector domain is referred to as pressure coupling. Further coupling mechanisms such as velocity or injector coupling are not considered here.

Herein, the single flame is subjected to an acoustic perturbation comparable to the multi-injector configuration. Due to the small ratio of injector to chamber diameter, an acoustic compactness assumption for the first transverse mode is allowed. Therefore, the single-injector domain is subjected to a defined harmonically oscillating pressure amplitude which is, however, approximately constant in the entire single-injector domain.

A real gas model is mandatory to describe O_2 which is injected at high pressure and low temperature. Here, the Redlich-Kwong equation of state is applied. However, H_2 and H_2O are treated as ideal gases. The specific heat capacities of O_2, H_2 and H_2O are evaluated using the NASA polynomials [14]. The transport properties, kinematic viscosity and heat conductivity are derived from the kinetic theory model.

3.3. *Linearized Euler Equations code: PIANO*

The stability analysis is carried out with the three-dimensional time-domain solver PIANO† which solves the Linearized Euler Equations. The code is based on a dispersion relation preserving 7-point stencil finite difference scheme (4th-order). The time integration is performed by a standard 4th-order Runge-Kutta scheme. A mean flow field, previously computed, must be given as an input for the simulation. An initial pulse is used to trigger the system. If a combustion response function, which gives a relation between heat release oscillation and acoustic pressure, is included, the thermoacoustic feedback can be investigated. An acoustically neutral energy boundary condition at the inlet is applied by setting acoustic mass flow fluctuation to zero in PIANO as presented in [17]. To be consistent with the meanflow computation, adiabatic slip conditions are applied to the walls. The supersonic flow condition in the divergent part of the nozzle

† Developed by the "Deutsches Zentrum für Luft- und Raumfahrt" (DLR), Prof. Delfs

	LP1	**LP2**	**LP3**	**LP4**
f_{T1}	10690	11360	11270	11270

TABLE 3. First transverse mode frequency for LP1-4 modes: results of the acoustic analysis carried out with PIANO

provides a natural anechoic end to the computational domain, which allows to apply any kind of boundary condition at the outlet of the configuration. For convenience, free slip conditions are used.

A classical n-τ model is implemented into PIANO to account for the combustion response [15, 16]. The following source term is included in the energy equation:

$$\dot{q}' = n\frac{\bar{\dot{q}}}{\bar{p}}\left[p'(t) - p'(t-\tau)\right] \tag{3.1}$$

where n is the interaction parameter and τ the time lag. A spatial distribution of the mean heat release $\bar{\dot{q}}$ can also be given to the code as an input.

4. Results

The coupled numerical procedure has been applied to investigate the BKD linear stability for the first transversal mode.

4.1. *Acoustic Analysis*

An acoustic analysis of the BKD has been carried out to evaluate the frequency of the first transversal mode, for the four load points. For that purpose, the PIANO code is used without feedback. The eigenfrequencies of the BKD, for a given load point, are determined by investigating the impulse response. To excite the acoustics, an initial pulse in form of an initial local acoustic pressure distribution with a Gaussian shape is used. The pulse is schematically represented by the sphere in Fig. 4. The pulse excites all the acoustic modes that can be extracted from the pressure time series. In Fig. 5 the acoustic pressure evolution in a monitor point is shown for LP1-3 cases (LP4 is very similar to LP3). The eigenfrequencies are extracted by a Fast Fourier Transform (FFT) of the signal, starting after the initial pulse decays. The FFT gains for LP1, LP2 and LP3 are shown in Fig. 5 (LP4 is very similar to LP3). The first and highest peak which appears in the FFT should correspond with the first transverse frequency: the values have been reported in Table 3. Note that longitudinal modes are not visible in these figures. This can be explained considering that the nozzle has a high damping effect on the longitudinal modes [18, 20].

4.2. *Single injector simulation: FTF determination*

Single injector unsteady simulations have been carried out with the models presented in Section 3.2. Goal of these simulations is the combustion response analysis and the extraction of a FTF around the frequency of the BKD first transverse mode. A FTF for a frequency range of $8000 - 11500$Hz with a resolution of $\Delta f = 500$Hz has been calculated for each load point. During each unsteady simulation the pressure close to the injector and the volumetric heat release rate, averaged over the whole domain, are monitored. A number of 15 acoustic periods are considered to compute the FTF which is defined

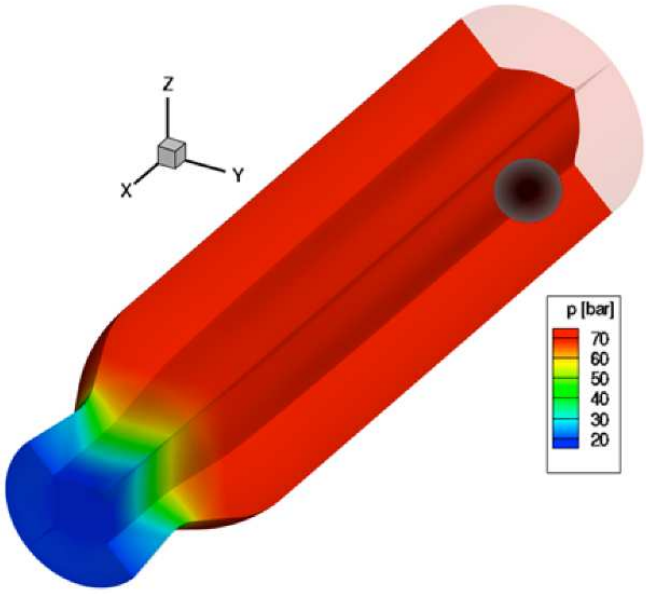

FIGURE 4. Domain, mean pressure field and excitation pulse used for the acoustic analysis of the LP1 case with PIANO

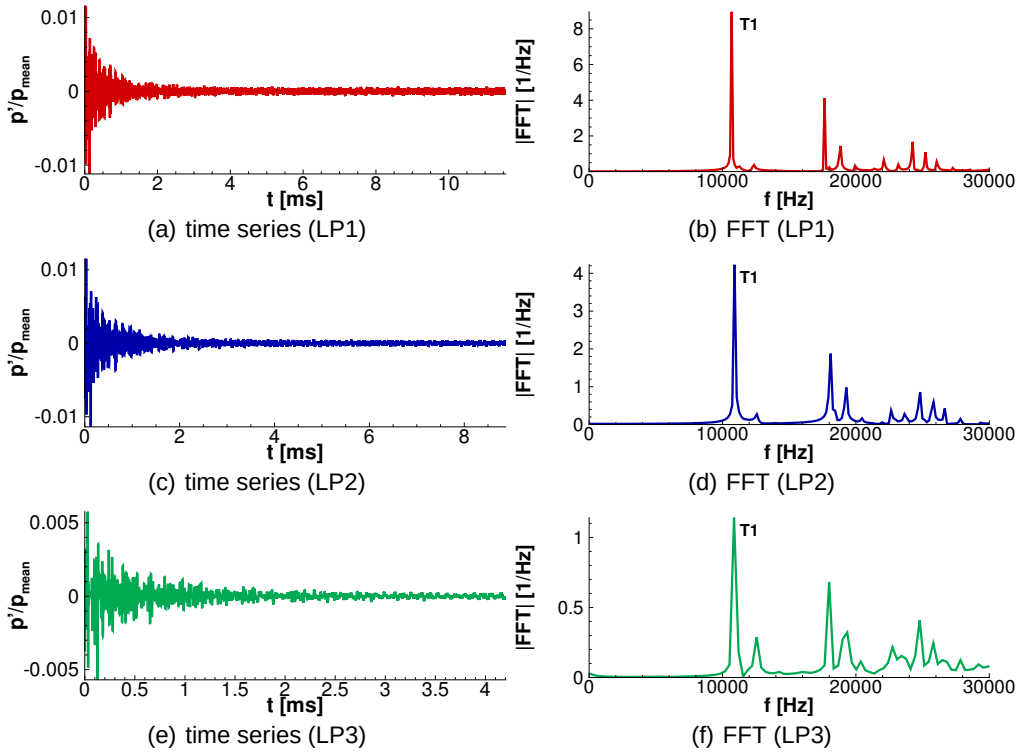

(a) time series (LP1) (b) FFT (LP1)

(c) time series (LP2) (d) FFT (LP2)

(e) time series (LP3) (f) FFT (LP3)

FIGURE 5. Acoustic analysis: PIANO results without feedback. Pressure time series and corresponding FFT for LP1-3 cases (LP3 and LP4 are similar)

	LP1	**LP2**	**LP3**	**LP4**
$\dot{Q}_{total}$ [MW]	58.9	76,7	87,0	86,9
$\lvert FTF\rvert_{\omega_{T_1}}$	1,289	1,171	1,141	1,132
$\phi_{\omega_{T_1}}$	1,260	0,505	0,094	0,453
$n_{\omega_{T_1}}$	2,105	0,669	0,573	0,630
$\tau_{\omega_{T_1}}$	$9,351 \cdot 10^{-6}$	$2,972 \cdot 10^{-5}$	$4,200 \cdot 10^{-5}$	$3,179 \cdot 10^{-5}$
RF	0,39	1,02	1,13	1,02

TABLE 4. Results of the single injector simulation: FTF Gain ($|FTF|$), FTF phase (ϕ), n and τ for LP1-4 evaluated at the frequency of the first transverse mode (T1).

by Eq. (1.1) in the frequency domain. In particular, for each frequency, gain and phase are evaluated from the time series, considering the ratio of amplitudes of the fluctuating quantities and the time lag between them, respectively.

The computed FTF have to be reduced to the classical n-τ formulation, given by Eq (3.1), which is included into PIANO as a source term (see Section 3.3). For this purpose, only the FTF values at the frequency of the first transverse mode are considered and the $n_{\omega_{T1}}$ and $\tau_{\omega_{T1}}$ values are evaluated by:

$$\tau_{\omega_{T1}} = \text{atan}[\tan^{-1}(\phi_{\omega_{T1}})]\frac{2}{\omega_{T1}} \tag{4.1}$$

$$n_{\omega_{T1}} = |FTF|_{\omega_{T1}} \frac{\sin(\phi_{\omega_{T1}})}{\sin(\omega_{T1}\tau_{\omega_{T1}})}. \tag{4.2}$$

The gain ($|FTF|$) and phase (ϕ) of the FTF at the frequency of the first transverse mode and the corresponding parameters n and τ for LP1-4 are summarized in Table 4. These parameters characterize the feedback in terms of an amplitude and a phase relation between pressure and heat release.

A first indicator of which load point can be expected to lead to the strongest feedback is given by the response factor RF, which is defined as:

$$RF = |FTF|_{\omega_{T1}} \cos(\phi_{\omega_{T1}}). \tag{4.3}$$

In fact the response factor takes into account both the interaction parameter between acoustic pressure and heat release and their phase. The computed response factors for each load point, at the T1 frequency, are shown in Table 4. LP2, LP3 and LP4 have similar response factors around 1 whereas LP1 has a response much lower, around 0.4. This indicates that a higher stability level for the first transverse mode is expected for LP1 than for the other load points. A slight difference can however be observed between the three last load points, LP3 showing the highest response factor which is essentially explained by the small phase value of LP3. In other words, pressure and heat release are most in-phase for LP3 than for the other load points. On the other hand, LP2 and LP4 show similar values for amplitude and phase which translates to a similar response factor lower than the LP3 one. In conclusion, the FTF of LP3 shows the highest potential to amplify acoustic amplitudes in the thermoacoustic feedback system.

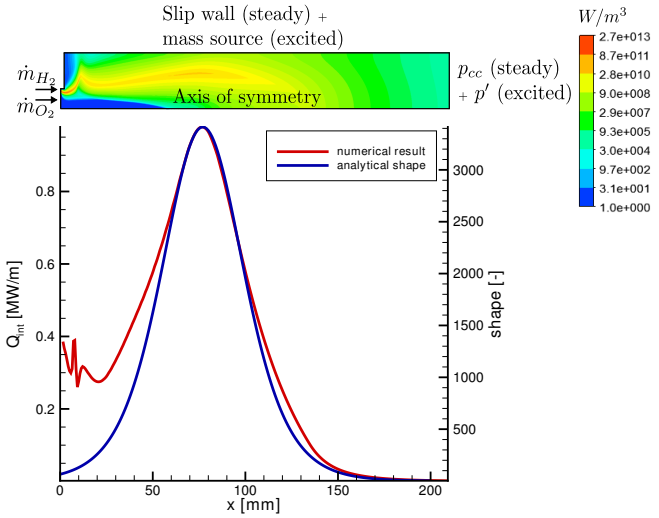

FIGURE 6. Top: single injector simulations domain and boundary conditions with the resultant volumetric heat release rate (logarithmic scale) for LP3. Bottom: radially integrated volumetric heat release distribution in the axial direction and analytical shape function.

The steady field solution for each load point is used to extract a spatial distribution of the heat release which is necessary to include a realistic distribution of the feedback source term in the PIANO simulation. For this purpose, the heat release rate is integrated in the radial direction and an analytical function which matches the axial distribution is derived. The shape function, shown in Fig. 6, is defined to be zero at the inlet to ensure a well-defined zero acoustic mass flow boundary condition in PIANO (see Section 3.3). Additionally, Fig. 6 shows the distribution of the volumetric heat release rate on a logarithmic scale. The highest values are observed at an axial position of about 80 - 85 mm.

The total heat release rate $\dot{Q}_{total}$, averaged over the single injector domain, has also been extracted from the simulations for the different load points and is reported in Table 4. The highest heat release rates are obtained for the two 80 bar pressure cases (i.e. LP3 and LP4).

4.3. *Thermoacoustic feedback analysis*

The thermoacoustic feedback analysis of the BKD is done with PIANO, keeping the same numerical setup that has been used to carry out the acoustic analysis without feedback (see Section 4.1), that is initially exciting the system with a Gaussian pressure distribution to obtain a a randomly distributed white noise acoustic field and then observing the time series evolution. Moreover, the FTF computed with the single injector simulation is included into the feedback source term in the energy equation through the $n-\tau$ parameters evaluated as described in Section 4.2. However, the feedback term is not activated from the beginning of the simulation. Rather, the feedback loop is turned on only after the acoustics are well distributed over the entire domain. That is, in the present conditions, after about 1.2ms. The stability of the configuration is then judged determining the growth rate of the first transverse mode from the monitored time series of pressure at an arbitrary position within the chamber.

The time series of the pressure in one monitor point are shown in Fig. 7 for all the load

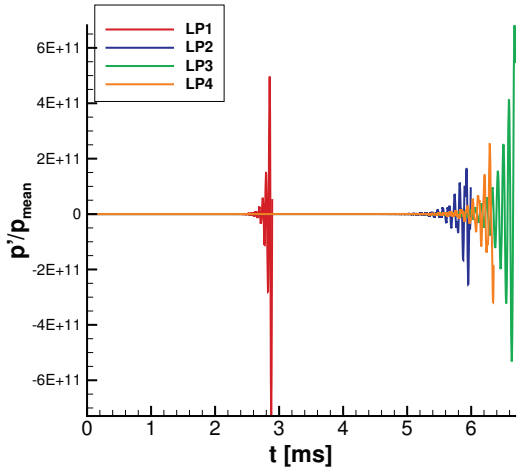

FIGURE 7. Recorded pressure signal in the combustion chamber with feedback. The feedback is turned on after about 1.2ms.

points. It is clearly visible that all load points show amplified pressure amplitudes and LP1 in a shorter time. A frequency analysis shows that the main oscillation frequency for LP2-4 corresponds to the T1 frequency as demonstrated by the FFT gain plots of Fig. 9. That is in agreement with the calculated response factors, reported in Table 4, which are all positive. The BKD chamber is not equipped with additional damping devices such as absorbers or baffles. Therefore, in the linear modelling presently used, the only damping mechanism considered is the damping by the nozzle. Viscous damping is considered to be negligible. However, the acoustic properties of the nozzle lead to a strong damping of longitudinal modes, whereas transverse modes get damped weakly, as observed in the acoustic analysis of Section 4.1 and in literature [18, 20]. This explains why a positive response factor of all load points leads to growing pressure amplitudes, as it is observed in Fig.7.

A different situation is observed for LP1 for which the higher contribution is obtained at the T2 frequency as shown by its FFT in Fig. 9. The T2 mode dominates over the T1 and thus the comparison with the other load points is not feasible. The T2 contribution is not of interest in the present analysis which focuses on the T1 mode. However, in the framework of testing the whole coupled numerical procedure, it is interesting to understand the observed behavior. The T2 contribution does not come from the FTF, that has been considered only for the T1 mode, rather it is the consequence of a inherent issue in the n-τ model. This can be explained by the frequency description of the n-τ model of Eq. (3.1), which reads:

$$\hat{q} = \bar{q} n (1 - \exp(i\omega\tau)) \frac{\hat{p}}{\bar{p}} \tag{4.4}$$

which is shown in Fig. 8 for each load point. The gain and phase for the T1 mode correspond to the values determined in the flame response identification procedure in the single-injector simulation. These are the only values of interest in the present analysis. However, gain and phase of the function given by Eq. (4.4) assume some values also in the rest of the frequency range. Incidentally, the gain and phase behavior at the T2 frequency significantly differs between LP1 on one hand and LP2-4 on the other hand. The n-τ model provides both a higher gain and a smaller phase difference between

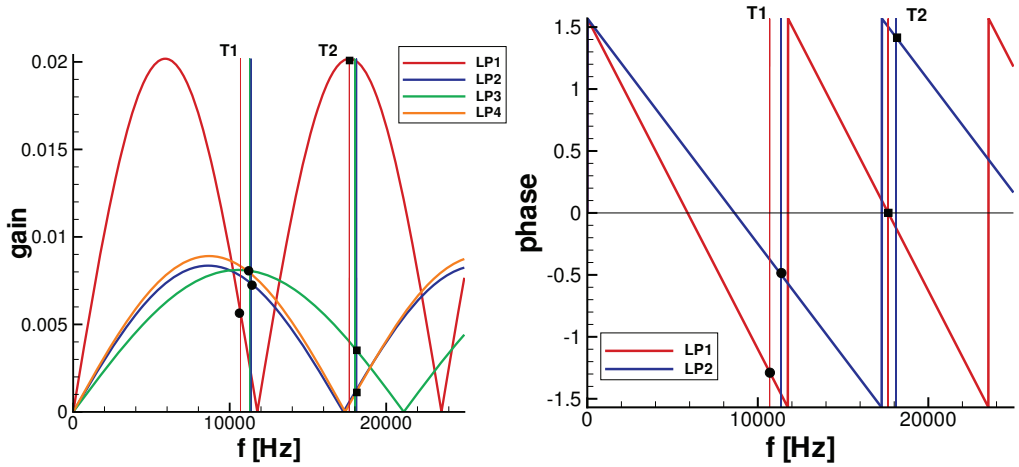

(a) gain (b) phase

FIGURE 8. Frequency description of the n-τ model in terms of gain for LP1-4 and phase for LP1-2. Circles and squares indicate the response at the T1 and T2 mode frequencies respectively.

pressure and heat release fluctuations for LP1. The corresponding LP1 response factor for T2 is significantly higher than for T1. For LP2-4 that is not the case.

In general, the behavior of the T2 and higher modes are not of interest and do not affect the result of the T1 mode in this linear model. However, the artificial feedback and therefore growth of the T2 amplitude for LP1 is so strong that it dominates the acoustic field and hence obscures the result for the T1 mode. In fact, the monitored time series leads to unrealistically high amplitudes in a very short time. Therefore, the LP1 time series is not suitable to carry out a spectral analysis since it is not possible to extract the T1 mode from it.

The chosen n-τ modelling of the feedback is therefore not suitable to investigate the growth of LP1 in more detail. However, judging from the response factors reported in Table 4, LP1 should give the weakest response of all load points.

The growth rates for LP2-4 are determined through a gliding FFT investigation. In this procedure, the time series is split into time windows with equal length. For each time window a FFT is performed. By assuming an exponential decay of the amplitude, the growth rate can be evaluated by fitting an exponential ansatz function to the changing mode amplitudes. In Fig. 10 the gliding FFT is shown for LP2: similar figures are obtained for LP3 and LP4 (not shown here). The gliding FFT procedure allows to distinguish between the growth rates of the different acoustic modes. In the context of the presented methodology, only the growth rate of the first transverse mode is of interest. In the present analysis, three time windows for the gliding FFT are used. The evaluated growth rates for LP2-4 are summarized in Table 5. Contrary to expectations, LP3 shows the lowest growth rate and LP2 the highest. However, the differences are rather small and can be explained by the similar response factors values.

5. Conclusions and future tasks

A coupled methodology has been tested to evaluate the linear combustion stability of a given rocket engine configuration. For the procedure, only the geometry and load

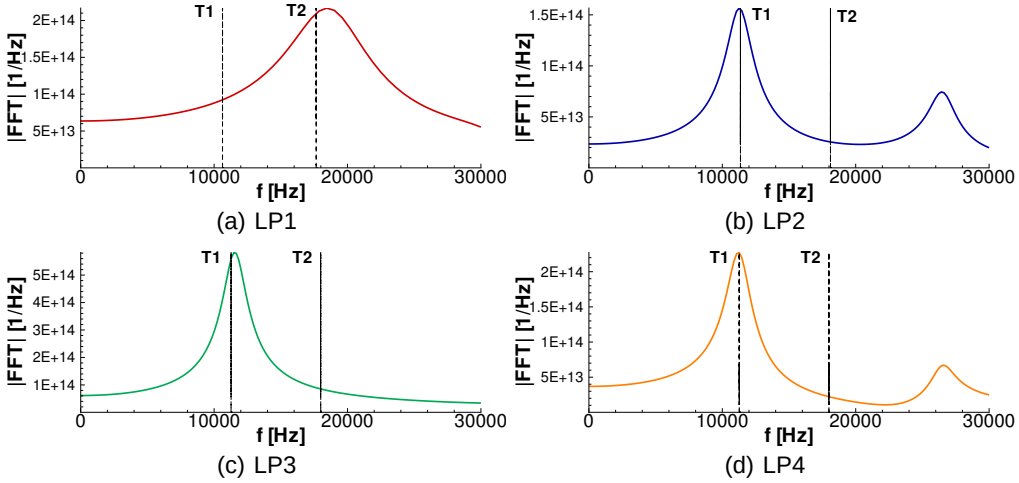

FIGURE 9. Thermoacoustic feedback analysis: FFT of the non dimensional pressure for LP1-4 cases. Vertical lines indicate T1 and T2 acoustic modes frequencies.

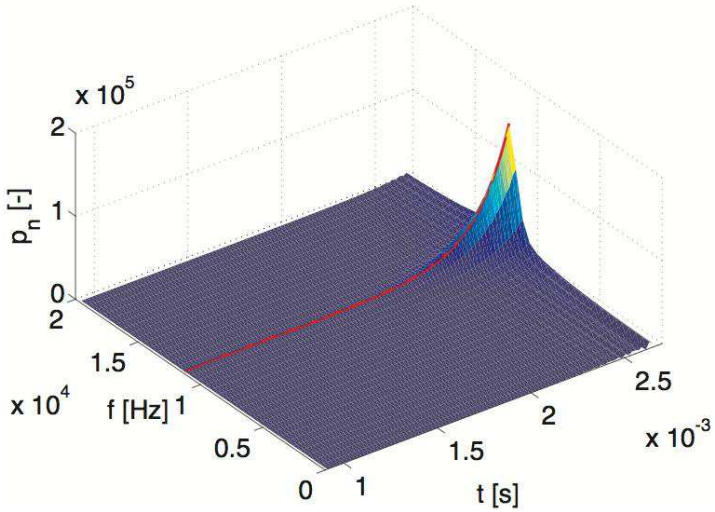

FIGURE 10. Gliding FFT for LP3. The red line indicates the exponential behavior of the T1 mode amplitude. LP2 and LP4 are similar.

	LP1	**LP2**	**LP3**	**LP4**
Growth rate [1/s]	-	6350	5750	5950

TABLE 5. Computed growth rates for the T1 mode for LP2-4

point conditions in terms of chamber pressure, mass flows of propellants and their injection temperatures are required. The flame response is determined in a single-injector setup which is based on an unsteady RANS simulation with a standard Eddy-Dissipation modelling of the combustion process and real gas treatment for the oxygen. The acous-

tic compactness assumption for the flame allows to characterize the flame response to transverse excitation. Here, a direct pressure coupling is considered as coupling mechanism between pressure and heat release exclusively. The stability analysis is performed in a succeeding step with the time-domain code PIANO, which solves the linearized Euler equations. Herein, the flame feedback is included in form of the classical n, τ model as source term in the energy equation. A gliding FFT of the time series finally determines the growth rates and allows to identify the load point with the highest potential to show an unstable behavior.

As a test case, DLR's BKD chamber operated at four different load points is used. It shows self-excited instabilities under representative load point conditions for the propellants H_2/O_2. The high chamber pressure and low injection temperature of O_2 requires a real gas treatment.

Results show that LP3 has the highest response factor and LP1 the lowest one. However, the response factors of LP2 and LP4 are similar compared to LP3. From the stability investigations, LP2-4 also shows rather similar growth rates. However, LP2 can still be identified with the highest growth rate, which is contradictory to the calculated response factors. The small differences in growth rates could also be explained by insufficient large time series used for the evaluation of the gliding FFT.

The stability of the first transverse mode for LP1 could not be judged because the applied n, τ model comprises an inherent amplification at different frequencies as well. In particular, for the LP1 case, the applied n, τ model leads to a strong amplification of the second transverse mode. As a consequence, in the time series the first transverse mode cannot be identified.

Altogether, the general applicability of the methodology could be shown. Linear stability investigations are possible from only the knowledge of the geometry and the load point conditions.

In the future, a more advanced modelling of the feedback is required to allow for stability analysis of all load points. In terms of flame response characterization, different coupling mechanisms between the acoustics and heat release must be considered to capture the feedback in more detail. The stability analysis in PIANO needs to be extended to also include relevant subcomponents as e.g. the feed- and injection system and absorbers. Especially the damping characteristics must be incorporated into the stability analysis. More advanced post-processing techniques as POD and DMD will support the understanding of the thermoacoustic feedback phenomena.

Acknowledgments

Financial support has been provided by the German Research Foundation (Deutsche Forschungsgemeinschaft – DFG) in the framework of the Sonderforschungsbereich Transregio 40. Computational resources have been provided by the Leibniz-Rechenzentrum München (LRZ). PIANO is provided by the DLR Braunschweig, Prof. Delfs.

References

[1] PRIEM, R. J. (1997). *Guidlines for Combustion Stability Specifications and Verification Procedures for Liquid Propellant Rocket Engines*. Chemical Propulsion Information Agency.

[2] HARRJE, D. AND REARDON, F. (1972). Liquid Propellant Rocket Combustion Instability. *NASA SP-194*.

[3] CULICK, F. AND YANG, V. (1995). *Overview of Combustion Instabilities in Liquid-Propellant Rocket Engines*. American Institute of Aeronautics and Astronautics.

[4] YANG, V. AND ANDERSON, W. (1995). Liquid Rocket Engine Combustion Instability. *Progress in Astronautics and Aeronautics*, **169**, AIAA, Washington, D.C..

[5] GRÖNING, S. AND OSCHWALD, M. (2013). *LOX/H2-Combustion with self-sustained acoustic excitation*. HF-7 test case description, 3rd REST† Workshop on Combustion Instability Modelling.

[6] GRÖNING, S., OSCHWALD, M. AND SATTELMAYER, T. (2012). *Selbsterregte tangentiale Moden in einer Raketenbrennkammer unter repräsentativen Bedingungen*. Deutscher Luft- und Raumfahrtkongress, Berlin, Germany, 2012.

[7] GRÖNING, S., SUSLOV, D., OSCHWALD, M. AND SATTELMAYER, T. (2013). Stability behavior of a cylindrical rocket engine combustion chamber operated with liquid hydrogen and liquid oxygen. *5th European Conference for Aeronautics and Space Sciences*, Munich, Germany, 2013.

[8] SCHULZE, M., SCHMID, M., MORGENWECK, D., KÖGELMEIER, S. AND SATTELMAYER, T. (2013). A Conceptional Approach for the Prediction of Thermoacoustic Stability in Rocket Engines. *49th AIAA/ASME/SAE/ASEE Joint Propulsion Conference*, San Jose, California, USA, 2013.

[9] GLENN RESEARCH CENTER. *Chemical Equilibrium with Applications*. http://www.grc.nasa.gov/WWW/CEAWeb/

[10] SCHMID, M. AND SATTELMAYER, T. (2011). Influence of Pressure and Velocity Perturbations on the Heat Release Fluctuations for Coaxial GH2/GO2 Injection. *4th European Conference for Aerospace Sciences*, St. Petersburg, Russia.

[11] SCHMID, M. AND SATTELMAYER, T. (2012). Interaction of Acoustic Pressure Fluctuations with Supercritical Nitrogen Jets. *48th AIAA/ASME/SAE/ASEE Joint Propulsion Conference & Exhibit, AIAA 2012-3858*, Atlanta, Georgia, USA.

[12] RAMCKE, T., SCHMID, M. AND SATTELMAYER, T. (2013). Response Characterization of a LOX-GH2 Flame to Forced Acoustic Pressure Fluctuations. *5th European Conference for Aeronautics and Space Sciences, München, Germany*.

[13] SCHMID, M., BLUMENTHAL, R. S., SCHULZE, M., POLIFKE, W. AND SATTELMAYER, T. (2013). Quantitative Stability Analysis Using Real-Valued Frequency Response Data. *Proceedings of ASME Turbo Expo, No. GT2013-95459*, San Antonio, Texas, USA.

[14] BURCAT, A. (1984). Thermochemical Data for Combustion Calculations. Chapter 8 of *Combustion Chemistry*, Gardiner, W. C. (Ed.), Springer-Verlag, New York.

[15] CROCCO, L. AND CHENG, S. (1956). *Theory of Combustion Instability in Liquid Propellant Rocket Motors*. Butterworth Scientific Publications.

[16] PIERINGER, J. (2008). *Simulation selbsterregter Verbrennungsschwingungen in Raketenschubkammern im Zeitbereich*. Ph.D. thesis, Technische Universität München.

[17] MORGENWECK, D., PIERINGER, J. AND SATTELMAYER, T. (2010). Numerical determination of nozzle admittances in rocket engines. *New Results in Numerical and Experimental Fluid Mechanics VII, Notes on Numerical Fluid Mechanics and Multidisciplinary Design*, **112/2010**, 579–586.

[18] KATHAN, R., MORGENWECK, D., KAESS, R. AND SATTELMAYER T. (2010). Validation of the Computation of Rocket Nozzle Admittances with Linearized Euler Equations. *4th European Conference for Aerospace Sciences*.

† Rocket Engine Stability Research Initiative

[19] MORGENWECK, D., FASSL, F. AND SATTELMAYER, T. (2009). Influence of Scaling Rules on the Loss of Acoustic Energy through Demonstrator Rocket Nozzles. *SFB/TRR 40 – Annual Report 2009*.

[20] SCHULZE, M., GIKADI, J. AND SATTELMAYER, T. (2013). Acoustic Admittance Prediction of Two Nozzle Designs of Different Length Using Frequency Domain Simulations. *5th European Conference for Aeronautics and Space Sciences*, Munich, Germany.

[21] SUTTON, G. P. AND BIBLARZ, O. (2001) *Rocket Propulsion Elements*. John Wiley and Sons, seventh edition.

[22] MCBRIDE, B. J. AND GORDON, S. (1994). Computer Program for Calculation of Complex Chemical Equilibrium Compositions and Applications, National Aeronautics and Space Administration, Lewis Research Center, Cleveland, Ohio, 44135-3191, October 1994, Reference Publication, *NASA RP-1311.*